Catalysis Today 359 (2021) 90–98

Contents lists available at ScienceDirect

Catalysis Today

journal homepage: www.elsevier.com/locate/cattod

Modeling the triple-path electro-oxidation of formic acid on platinum: Cyclic voltammetry and oscillations

Alfredo Calderón-Cárdenas[a,b,*], Fabian W. Hartl[a], Jason A.C. Gallas[c,d,e], Hamilton Varela[a,c,*]

[a] Instituto de Química de São Carlos, Universidade de São Paulo, CEP 13560-970, São Carlos, SP, Brazil
[b] GIFBA, Universidad de Nariño, A.A.1175, San Juan de Pasto, Nariño, Colombia
[c] Max-Planck Institute for the Physics of Complex Systems, D-01187, Dresden, Germany
[d] Complexity Sciences Center, 9225 Collins Avenue Suite 1208, Surfside, FL, 33154, USA
[e] Instituto de Altos Estudos da Paraiba, Rua Silvino Lopes 419-2502, 58039-190, João Pessoa, Brazil

ARTICLE INFO

Keywords:
Formic acid
Electro-oxidation
Oscillations
Mechanism
Modeling
Numerical simulations
Platinum
Electrocatalysis

ABSTRACT

A renewed electrochemical model for the oscillatory electro-oxidation of formic acid on platinum in acidic medium is presented. The model includes recently reported mechanistic findings and evaluates three reaction pathways towards the production of CO_2. Two of these processes consist of dehydrogenation and dehydration of the formic acid with adsorbed formate species as common intermediate. The third and most active pathway includes a fast oxidation of the formate ion. The proposed mechanism is translated into a kinetic model and tested in numerical simulations under voltammetric and oscillatory regimes. Numerical results are further compared with experimental ones. A successful adjustment of the oscillatory characteristics, namely frequency and amplitude of the oscillations suggest a good approximation to the actual mechanism of the oxidation of formic acid on platinum. The role of electrochemical oscillations in mechanistic studies is discussed and a comparison with previous models is also provided. Finally, some perspectives are suggested.

1. Introduction

The formic acid (FA) electro-oxidation reaction (FAEOR) is an important reaction in energy conversion, since formic acid can be applied directly in polymer electrolyte membrane fuel cells (PEMFCs) [1], and also occurs as a reaction intermediate in the oxidation of methanol, which is the most studied fuel for PEMFCs [2,3]. Thus, understanding the FA oxidation mechanism, as well as the factors that affect its reaction kinetics, is of great importance for the design of cost-efficient anode catalysts for PEMFCs and to optimize the electrocatalysis in the electro-oxidation of small organic molecules used as fuels [4].

Different mechanisms for the FAEOR on platinum have been proposed since the 70 s which have often been reevaluated according to insights from both spectroscopic experiments [5–17] and theoretical calculations using the density functional theory (DFT) [18–22]. A first plausible mechanism for the FAEOR on platinum, that consisted of direct and indirect pathways, was proposed by Capon and Parsons [23]. The direct path involves a fast reaction via a reactive intermediate, which is immediately oxidized further to CO_2. Initially, COOH species (bonded by the carbon atom) was reported as a possible candidate [23], but no spectroscopic evidence in this direction could be found reproducibly. Osawa and co-workers proposed formate in a bridge-bonded configuration, i.e. bonded via both oxygen atoms to two surface sites ($HCOO_B$), as a reactive intermediate in the direct pathway of the FAEOR on platinum electrodes [7–9]. The other pathway includes a step that an inhibiting intermediate is formed and impedes further adsorption of FA. For this indirect pathway, CO_{ads} was identified unequivocally as the poisonous species [25–27]. Fig. 1 shows a scheme of this mechanism.

Yet, the dual pathway mechanism and the role of the bridge-bonded formate as active intermediate were discussed controversially [15]. One important argument is that the faradaic current observed experimentally increases faster than the coverage of bridge-bonded formate in chronoamperometric measurements with different formic acid concentrations. This indicates that adsorbed bridge-bonded formate cannot be considered as a reaction intermediate in the dominant reaction pathway [10–12]. Considering that the formate is a spectator rather than a reactive intermediate, some authors proposed a third pathway in the reaction mechanism of the FAEOR [8,10–12,31,34,35]. Nevertheless, studies using improved infrared techniques which allowed to monitor the dynamics of electrode reactions (time-resolved Surface-Enhanced Infrared Absorption Spectroscopy - SEIRAS) [6–8,15] and

* Corresponding authors at: Instituto de Química de São Carlos, Universidade de São Paulo, CEP 13560-970, São Carlos, SP, Brazil.
E-mail addresses: alfredocalderon@udenar.edu.co (A. Calderón-Cárdenas), hamiltonvarela@usp.br (H. Varela).

https://doi.org/10.1016/j.cattod.2019.04.054
Received 1 February 2019; Received in revised form 28 March 2019; Accepted 14 April 2019
Available online 15 April 2019
0920-5861/

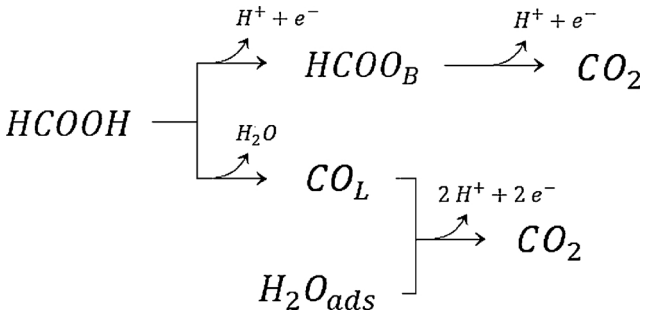

Fig. 1. Scheme of the dual-pathway mechanism for the FAEOR on platinum. (Adapted from reference [28]).

DFT calculations indicate that $HCOO_B$ [18,20,21,36] can be an active intermediate in the FAEOR. Another aspect under discussion in the elucidation of the mechanism lies in specifying the contribution of formate ($HCOO^-$) in the overall reaction. John et al. suggested a dual pathway mechanism for the $HCOO^-$ oxidation [37]. Joo et al. studied the FAEOR in a wide pH range and proposed that the formate ion is the major reactant even in strong acidic media [32]. Thus, the increased oxidation current with pH can be explained considering a weakly adsorbed $HCOO^-$ as a precursor [32,38]. Therefore, the experimental observations corroborate the involvement of solution formate in the oxidation process [18,39].

In addition to conventional studies, the kinetic modeling of the FAEOR, especially under oscillatory regime, can provide additional information about the electrode dynamics [17,40–44] and help in the understanding of the mechanism [28,35,43,45–48]. A prerequisite for the occurrence of oscillations is the interplay between positive and negative feedback loops in the reaction network [49]. The positive feedback is associated with the presence of a negative differential resistance (NDR) i.e. the behavior where an increment of the potential will cause a further increase of the potential in a process called autocatalysis. In this process, water plays a significant role and its adsorption becomes stronger and active surface sites are more blocked for increasing potential, inhibiting the electro-oxidation reaction [50]. The negative feedback loop is associated with the process where an increment of the potential will form surface oxidized that reacting with the poisoning CO_{ad} and thus, a decreasing the coverage of the blocking species will produce a further decrease of potential.

Based on the dual-pathway mechanism, Albahadily and Schell [45] modeled the FAEOR under oscillatory regime including 10 reaction steps with 7 variables. Whilst, Okamoto et al. [46] successfully simulated the potential oscillations with only 3 variables and 5 reactions steps, suggesting that even if many reaction steps are involved in the FAEOR, a limited number of reaction steps plays an essential role to find potential oscillations [28,35,46,51]. Strasser et al. established a kinetic model under potenciostatic control, which also includes the mass balance of the surface concentration of FA in 4 differential equations [43]. Mukouyama et al. [28] modeled potential oscillations during the FAEOR and proposed that adsorbed CO not only acts as a site-blocking species but also suppresses the decomposition of $HCOO_B$, whose interaction leads to the potential instabilities [28]. Unlike these models, Mei et al. [35] suggested that the direct pathway involves another intermediate different that $HCOO_B$ which requires the cleavage of O—H and C—H bonds in a third pathway, c.f. Fig. 2.

So far it is clear that the mechanism of oxidation of formic acid is still quite under debate. In this work, we present a kinetic model that rationalizes several reported mechanistic aspects and considers that the FAEOR occurs through three pathways towards the production of CO_2. However, the role of the adsorbed formate species is highlighted as a common intermediate in the dehydrogenation and dehydration of formic acid.

The proposed model incorporates recently reported mechanistic aspects, and was evaluated in terms of the similitude between the simulated and experimental data under voltammetric and oscillatory regimes. An important criterion followed to determine the kinetic parameters in our model was to set the charge transfer coefficients in values between 0.3 and 0.7 as expected in elementary reactions. In this way, this paper contributes to clear up the mechanism of oxidation of formic acid through an updated model according to recently provided experimental and computational insights.

2. Materials and methods

Initially, an reaction scheme was proposed for the FAEOR according to experimental observations [5–17,34] and first-principle simulations [18–22,36] described in the literature. Then, a kinetic model was defined by the mass balance of the concentration of the reactants on the electrode surface and the charge balance at the electrode surface. This model was constantly re-evaluated by modifying the kinetic equations and parameters to achieve the best possible congruence between the simulated and experimental results. The coupled differential equations were resolved numerically using the software Wolfram Research, Inc., Mathematica version 11.2, Champaign, IL (2017).

Regarding the experimental measurements, these were obtained with a conventional two-compartment, three electrode glass cell was used for all measurements. The working electrode (WE) was a platinum plate of about 0.3 cm^2 in geometric area with roughness of 1.2, which was flame annealed in a butane flame for about 30 s before entering the cell. The used reversible hydrogen electrode (RHE) was prepared in the same electrolyte, which was used for the characterization of the present system. A platinum foil of much greater area than that of the WE was used as counter electrode (CE). The measurements were carried out with an Autolab potentiostat/galvanostat PGSTAT 30. All potentials in this paper are quoted versus the RHE. The reference electrode was placed in the same compartment of the electrochemical cell. Solutions were prepared using sulphuric acid (97.3%, J.T. Baker), potassium sulphate (99.0%, Sigma-Aldrich), formic acid (98%, Sigma-Aldrich) and Milli-Q-water (18.2 MΩ cm). Before each experiment the solution was purged with argon (99.996%, White Martins) for at least 5 min. After an electrochemical annealing by cyclic voltammetry (CV) of at least 1000 cycles in the basic electrolyte in the potential range between 0.05 and 1.45 V and a scan rate of 1 V s^{-1}, a CV at 0.05 V s^{-1} was carried out in the same potential window to ensure the cleanliness of the system. Afterwards the electrode was put in a solution with the identical pH, containing the same ingredients and formic acid. Another CV at 0.05 V s^{-1} was performed to check the reproducibility of the characteristic features the voltammogram of formic acid oxidation on platinum before any further procedure.

3. Results and discussion

3.1. Reaction mechanism

Recent publications [18,20,52] have suggested the possibility that the $HCOO_L$ is an intermediate both in the formation of CO_{ad} on platinum and in the production of CO_2. It is also argued that monodentate adsorbed formate is quickly transformed to the much more favorable bidentate form. Therefore, it is reasonable to assume that the adsorption of FA produces $HCOO_B$ and that the active intermediate $HCOO_L$ is formed by the reversible configurational transformation from $HCOO_B$. Therefore, we proposed a preliminary reaction mechanism with two pathways and adsorbed formate species as common intermediates. In addition, we include a third pathway [8,10–12,34,35] to account for the current observed in the cyclic voltammetry, *vide infra*. Fig. 3 shows the reaction scheme proposed with triple-path electro-oxidation of formic acid. In the following we discuss the details of all individual steps.

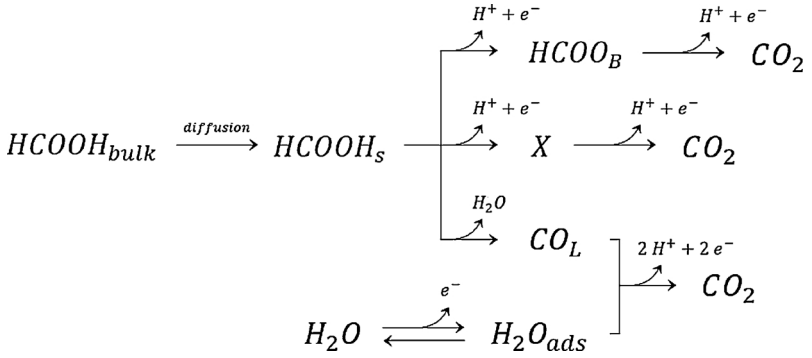

Fig. 2. Scheme of the triple-path mechanism for the FAEOR on platinum. (Adapted from reference [35]).

3.1.1. Formate pathway

The first pathway consists of the dehydrogenation process of FA as shown in equations *r1-r3*. The reactions involved are:

$$HCOOH + 2* \underset{-1}{\overset{1}{\rightleftarrows}} HCOO_B + H^+ + e^- \quad \text{(r1)}$$

$$HCOO_B + 2* \xrightarrow{2} HCOO_L + 3* \quad \text{(r2)}$$

$$HCOO_L + * \xrightarrow{3} CO_2 + H^+ + e^- + 2* \quad \text{(r3)}$$

where the asterisk represents a free surface reaction site, the 'B' and 'L' scripts indicate that the chemical species is adsorbed on the electrode surface in a bridge-bonded or linear-bonded configuration, respectively.

The reaction steps 1 and -1 indicated in equation *r1* correspond to fast adsorption of FA and desorption of $HCOO_B$ on and from the platinum surface, respectively [12,13,15–17,24,28,33,35,53]. By means of DFT Gao et al. proposed that the CO_2 formation is initiated by a single molecule of $HCOO_B$ in a process which involves a coupled proton-electron transfer [20,21]. However, $HCOO_B$ is not the species that forms CO_2 directly because the cleavage of the C—H bond requires high activation energy, above 1 eV [20]. Thus, step 2 is suggested as the rate-determining step (RDS). It is worth mentioning that Kibler and Al-Shakran [53] reported that the strongly bound $HCOO_B$ adsorbs in chain-like structures on Au(111) which achieves a phase transition characterized by a current jump with increasing potential.

Hence, the second step involves a configurational transformation of the adsorbed formate from a bridge-like adsorption mode to a monodentate one. The $HCOO_L$ has also been proposed as active intermediate even though it would be hindered by the presence of neighboring adsorbates [18]. This configurational change is necessary for activation of the C—H bond which requires an orientation with the hydrogen atom pointing to the metal surface [20]. This idea is also in agreement with results by Cuesta and Feliu's group who supposed that the reaction is mainly driven by the oxidation of monodentate formate [18,52]. Regarding the rotation of the adsorbed formate described by the equation *r2*, it should be noted that the presence of other neighboring adsorbed species prevents the process. Thus, it is plausible to assume that some neighboring free sites are required for the change of $HCOO_B$ to $HCOO_L$ configuration. In this case, we have assumed the requirement of two free sites per $HCOO_B$ molecule.

Finally, step 3 corresponds to the oxidation of $HCOO_L$ to CO_2 via the C—H-down configuration, where the C—H bond can be cleaved giving rise to the dehydrogenation with a lower activated energy [18,20].

3.1.2. Indirect pathway

For the second pathway evaluated, it is postulated that the CO_L formation also occurs from the intermediate $HCOO_L$. The proposed reaction is:

$$HCOO_L + H^+ + e^- + 2* \xrightarrow{4} CO_L + H_2O + 2* \quad \text{(r4)}$$

Early studies using infrared reflection absorption spectroscopy (IRAS) has undoubtedly shown that adsorbed CO is a poisoning species in the FAEOR [25–27,54]. However, unlike previous models [35], our proposal considers that the formation of CO_L on platinum can also proceed from monodentate adsorbed formate, i.e. after the reaction steps indicated in the equations *r1* and *r2*. This idea has been suggested at the solid-gas interface [55] and supported by experiments where a kinetic isotope effect has been ascribed to the faster decomposition of $HCOO_{ad}$ than $DCOO_{ad}$ [8]. Recent experiments and calculations using DFT also support this idea [18,20,21,36].

It is pertinent to clarify that the reaction described by equation *r4* does not correspond to an elementary reaction step. Some authors argued that, under any conceivable mechanism, the C—H bond should be broken, and that the adsorption mode should change from a Pt-O to a Pt-C binding mode [18]. However, if the first reaction step is the RDS, as suggested by DFT studies [18], then it can be considered that equation *r4* represents the overall kinetics of this process. This reaction requires two vacant sites [56] additional to the site required for the adsorption of $HCOO_L$. Thus, the CO_{ad} formation would require the presence of at least three contiguous Pt atoms according to the

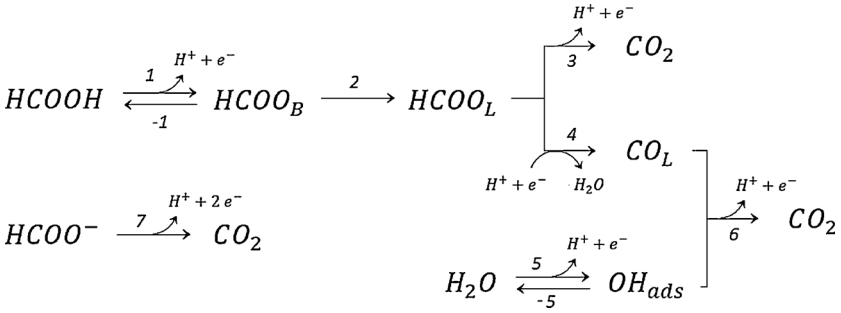

Fig. 3. Proposed reaction scheme for triple-path electro-oxidation of formic acid on platinum.

observation by Cuesta et al. [9] but the kinetic equation (Eq. (5)) corresponds to the reaction order 2 with respect to θ_{vac} [17,57].

On the other hand, the CO_{ad} formation rate decreases with increasing potential [7,39]. This behavior has been ascribed to potential-dependent changes in the concentration or orientation of the likely precursors of the HCOOH molecules and the $HCOO^-$ anions near the interface, or effects related to the polarity of the transition state for the CO_{ad} formation [10]. However, our model considers that the dehydration process (*r4*) is initiated by an electro-reduction process, which also can explain successfully the dependence on the potential of the formation of CO_L.

Regarding OH_{ad}, it is assumed that the oxygenated species on the surface of the electrode are formed from water at potentials from 0.50 V [58]. Here, we have not considered the formation of PtO_x, which are formed at higher potentials and subsequent to the adsorption of OH_{ad}. This is because the process of Eq. (5) is the predominant one in the simulated potential range and the inclusion of additional species does not significantly improve the results.

$$H_2O + * \underset{-5}{\overset{5}{\rightleftarrows}} OH_{ad} + H^+ + e^- + * \quad \text{(r5)}$$

In the potential range, where OH_{ad} is present, CO_L can be oxidized to CO_2 via Langmuir-Hinshelwood mechanism [46,59]. The electrochemical equation for CO_L oxidation can thus be expressed as:

$$CO_L + OH_{ad} \overset{6}{\rightarrow} CO_2 + H^+ + e^- + 2* \quad \text{(r6)}$$

3.1.3. Direct pathway

In this pathway, formate in solution is quickly oxidized to CO_2 by dehydrogenation:

$$HCOO^- + * \overset{7}{\rightarrow} CO_2 + H^+ + 2e^- + * \quad \text{(r7)}$$

If CO_{ad} is not present on the electrode surface and only the formate pathway is considered in the FAEOR, the faradaic current should be proportional to the $HCOO_B$ coverage. However, this is not experimentally observed [11,13,18,29] and because of that, Behm's group questioned the role of $HCOO_B$ as an intermediate. Since the contribution of dehydration pathway to the total current is negligible under the conditions mentioned, this observation requires the existence of another, third reaction pathway, which might be dominant without an IR-detectable adsorbed intermediate [10–12].

Regarding the nature of the chemical species that participates in the third pathway, DFT calculations of FA oxidation on the $Pt(111)/H_2O$ interface have shown that a possible reactive precursor is FA in a CH-down configuration [22]. It is worth mentioning that if this oxidation process involves the breakdown of the C–H bond in the RDS, the aforementioned kinetic isotope effect is to be expected, where the current densities for HCOOH are higher than those observed for DCOOH [10]. Experimentally, an ordered species containing a C═O vibrational mode at the interface with Pt(100) surface has been detected at moderate potentials where it also is observed significant oxidation current [60]. The authors employed advanced vibrational spectroscopic tools that provides the vibrational response of the first 1–2 layers of molecules at an interface in the presence of chemically identical molecules in the adjoining bulk liquid phase. Although formic acid was proposed as the molecule with the C═O vibrational mode by authors, this observation also makes it possible for the formate to be the precursor of the direct pathway. Recent studies on the pH effect on the FAEOR show an increasing current with increasing pH, suggesting that the active species in this pathway is the formate anion instead of formic acid [5,32,38]. In any case, this proposal does not invalidate the observed kinetic isotopic effect maintaining the idea that this oxidation process involves the breakdown of the C—H bond in the RDS. Another argument in favor of the anion formate being the active species in the third pathway has been discussed by Feliu's group [18]. If the RDS in this third pathway is a concerted proton-electron transfer, as would occur if HCOOH were the active species, then the equilibrium potential for the reaction should not shift in the RHE scale. However, it is observed experimentally that at pH > 3.75, where HCOOH is not the dominant species in solution, the onset potential shifting 40 mV per pH unit. Thus, this behavior suggests that the FAEOR happens through the reaction of formate anion to produce CO_2 [19].

Some studies using DFT show that if the anion approaches the surface with the C—H bond pointing towards the surface, occurs the C—H bond cleavage. In this process, there is no adsorption of the carbonaceous species but it does require free sites on the platinum surface for interaction with the H atom [19]. In conclusion, unlike from previous models [4,23,38], we consider that the active species in this third pathway is the formate anion instead of the formic acid that requires one free site to the dehydrogenation process.

According to the reaction steps proposed and their rate-determining steps, it is possible to establish the kinetic equations, which determine the rate of each process.

3.2. Kinetic equations

With the mechanism described above, we derive the following equations for the reaction rate of each step m -th: $v_m \equiv k_m(\phi) \prod_R (C_R \text{ or } \theta_R)$ [43,61,62] with $k_m(\phi)$ as the rate coefficient of the electrode reaction at potential ϕ, C_R the concentration of reactant R near the electrode surface, and θ_R as the coverage of an adsorbed reagent R on electrode surface. The coverage by the adsorbed species is defined as the ratio between the amount of adsorbed species and total surface sites.

Thus, the rate for FA adsorption and formate desorption, and the adsorbed formate oxidation can be expressed as following [8,28,35]:

$$v_1 = k_1(\phi)\, C_{HCOOH}\, \theta_{vac}{}^2 \quad (1)$$

$$v_{-1} = k_{-1}(\phi)\, \theta_{HCOO_B} \quad (2)$$

$$v_2 = k_2\, \theta_{HCOO_B}\, \theta_{vac}{}^2 \quad (3)$$

$$v_3 = k_3(\phi)\, \theta_{HCOO_L}\, \theta_{vac} \quad (4)$$

where θ_{vac} is the fraction of vacant sites defined as $\theta_{vac} \equiv (1 - \theta_{CO_L} - 2\theta_{CO_B} - \theta_{HCOO_L} - 2\theta_{HCOO_B} - \theta_{OH})$. In this work, it has been considered that the relationship between CO_L and CO_B maintain close to the equilibrium in which $\theta_{CO_B} \approx 0.258\, \theta_{CO_L}$. This ratio follows a coverage at saturation of 0.66 and 0.17 for CO_L and CO_B, respectively [17]. On the other hand, θ_{CO_B} and θ_{HCOO_B} are multiplied by 2 in the expression of θ_{vac} because each molecule occupies two surface sites. On the other hand, we have not considered the presence of other adsorbed species, for example, anions such as HSO_4^- or SO_4^{2-}, for the sake of simplicity [39]. Therefore, the simulation implicitly includes part of this effect in the parameters considered.

The rate for CO formation, water adsorption and desorption, and CO oxidation can be expressed as follows:

$$v_4 = k_4(\phi)\, \theta_{HCOO_L}\, \theta_{vac}{}^2 \quad (5)$$

$$v_5 = k_5(\phi)\, C_{H_2O}\, \theta_{vac} \quad (6)$$

$$v_{-5} = k_{-5}(\phi)\, \theta_{OH} \quad (7)$$

$$v_6 = k_6(\phi)\, \theta_{CO_L}\, \theta_{OH} \quad (8)$$

While the rate for the process described by equation *r7* can be written as:

$$v_7 = k_7(\phi)\, C_{HCOO^-}\, \theta_{vac} \quad (9)$$

In the above equations, the concentration of FA and formate in solution are determined as a function of pH in the bulk solution. Thus, we used the values of 1.99×10^{-1} M and 3.55×10^{-4} M as molar concentration for HCOOH and HCOO-, respectively. These

concentrations in the bulk at pH = 1.0 are assumed equal to double layer region and correspond to the nominal concentration of $C_{HCOOH} = 0.20$ M. The concentration of water in the double layer region equals its bulk concentration, which is constant during FA oxidation and assumed as $C_{H_2O}^{sup} \approx C_{H_2O}^{bulk} = 55$ M.

According to the Butler-Volmer theory, the rate constants are given by the expression $k_m(\phi) = k_m^0\, e^{\frac{\beta_m F}{RT}(\phi-\phi_m^0)}$ for oxidation reactions and by $k_{-m}(\phi) = k_{-m}^0\, e^{-\frac{(1-\beta_m)F}{RT}(\phi-\phi_m^0)}$ for the reverse reactions, with k_m^0 as the standard rate constant, β_m the charge transfer coefficient, F the Faraday constant, R the ideal gas constant, T the temperature, and ϕ_m^0 the standard potential of the reaction m. For convenience, the rate constants for the elementary steps are expressed as:

$$k_m(\phi) = e^{\frac{\beta_m F}{RT}(\phi-\phi_m)} \text{and}\; k_{-m}(\phi) = e^{-\frac{(1-\beta_m)F}{RT}(\phi-\phi_{-m})} \tag{10}$$

where $\phi_m = \phi_m^0 + \frac{RT}{\beta_m F} ln\left(\frac{1}{k_m^0}\right)$ and $\phi_{-m} = \phi_m^0 - \frac{RT}{(1-\beta_m)F} ln\left(\frac{1}{k_{-m}^0}\right)$.

According to the free energy curves for kinetics of electrode reactions, the most probable values for charge transfer coefficients are around of $\beta_m = 0.5$ due to the approximate symmetry of the energy barrier in elementary reactions. It turns out to lie between 0.3 and 0.7 in most systems [63]. Thus, terms $\frac{\beta_m F}{RT}$ and $\frac{(1-\beta_m)F}{RT}$ in the kinetic coefficients turn out to lie between 11.7 and 27.2 at 25 °C, respectively. One of the drawbacks of some previous models is that values used are not in the mentioned range. For example, values of $\frac{\beta_2 F}{RT} = 6.1$ and $\frac{\beta_3 F}{RT} = 5$ have been assumed [28], which result in $\beta_m = 0.16$ and 0.13, respectively.

It has been also assumed [28,35] the transfer of two electrons for the equivalent process to reaction *r6* in our model. This entails assuming a value of 39 for the term $\frac{\beta_m F}{RT}$. However, in our case reaction *r6* involves the transfer of a single electron. Thus, in this work all charge transfer coefficients have been set at a value of 0.5 except for the formation of oxygenated species and its reverse step which are not elementary reactions, and β_m reads 0.65.

Regarding the parameters ϕ_m and ϕ_{-m}, these were fitted to reproduce the observed oscillations and the voltammetry response, as indicated in Table 1. Finally, since reaction step *r2* is chemical and thus, does not depend on the potential as in Eq. (10), the rate coefficient of this step was also adjusted to reproduce the oscillations observed. The numerical values of the individual rate constants are further discussed below.

3.3. Kinetic model for the formic acid electro-oxidation

The kinetic model for the FAEOR can be defined by the mass balances of the concentration of the reactants on the electrode surface θ_R. The time-dependent change of θ_R is equal to the difference between the rate for the supply of R and the rate for its consumption through electrode reaction. Thus, one can write the equation for the evolution of $HCOO_B$, $HCOO_L$, CO_L, and OH_{ad} as following:

$$\frac{d\theta_{HCOO_B}}{dt} = v_1 - v_{-1} - v_2 \tag{11}$$

$$\frac{d\theta_{HCOO_L}}{dt} = v_2 - v_3 - v_4 \tag{12}$$

$$\frac{d\theta_{CO_L}}{dt} = v_4 - v_6 \tag{13}$$

$$\frac{d\theta_{OH}}{dt} = v_5 - v_{-5} - v_6 \tag{14}$$

A further differential equation is necessary to solve the system of nonlinear equations. This equation results from the charge balance at the electrical surface, which depends on the type of electrochemical experiment. For a galvanostatic experiment, the current applied to the electrochemical system i_{app} corresponds to the sum of the current of the faradaic and capacitive processes, i_F and i_C, respectively. The current density of the non-faradic processes can be expressed as $j_C = C_d \frac{d\phi}{dt}$, where C_d is the capacitance associated to the electric double layer and ϕ the potential difference between the electrode and the solution. The total faradaic current density corresponds to the sum of the current densities of each process, $j_F \equiv \sum_m F N_{tot} v_m$. Where, v_m is the rate of the m -th reaction step and N_{tot} are the total surface sites at the electrode by area unit. In the case of step 7, the current density considers the transfer of 2 electrons and consequently, can be written as $j_7 = 2F N_{tot} v_7$ [35]. Thus:

$$C_d \frac{d\phi}{dt} = j_{app} - F N_{tot} (v_1 - v_{-1} + v_3 - v_4 + v_5 - v_{-5} + v_6 + 2v_7) \tag{15}$$

Under potential control, c.f. the case of voltammetry experiments, instead of j_{app}, the term $\frac{E-\phi}{A R_s}$ is used [28], with E as the applied voltage between the reference electrode and working electrode, A is the electroactive area, and R_s is the electrical resistance. The values of the constants used in the numerical simulations are reported in Table 2.

The values for the total resistance and the double layer capacitance were estimated according to the size of electrochemical cell used in studies of voltammetry and chronopotentiometry of the FAEOR on Pt [38]. We used the electroactive area estimated via the electrochemical charge in the hydrogen region. The value for N_{tot} corresponds to the atomic density in a clean polycrystalline surface of platinum. This value was determined by the charge density of 210 $\mu C\, cm^{-2}$ for the monolayer hydrogen adsorption/desorption [17]

3.4. Voltammetric response

The electrochemical response that predicts the proposed model must be compared with different experiments in order to validate it. Thereby, we compared the results not only in the oscillatory regime but also with the voltammetric behavior. The following figure shows the simulated voltammetric profiles for the oxidation of formic acid and the coverages of adsorbates during this process. Additionally, experimental results reported previously have been included for comparison purposes.

Two oxidation peaks (I and II) appear along the positive-going scan and two peaks appears (IV and V) in the negative-going scan. Peaks are named according to the currently adopted nomenclature [5,23,64]. According to previous reports [5,64], in all peaks shown in the voltammetry of Fig. 4(a) there is an important contribution of the oxidation by the direct pathway. Additionally, peak II also has a small contribution of the CO_{ad} oxidation process to the total current which is less than 1% at room temperature [11–13,16,17,30,56]. Regarding the formate pathway, the contribution to the overall oxidation process is also very low. Therefore, almost all the faradaic current observed during the voltammetry corresponds to the process of oxidation of formate by the direct pathway. This idea is consistent with the appearance of a broad region of high current densities between 0.50 V and 0.70 V observed both forward and backward scan in quasi-stationary

Table 1
Kinetics parameters used in the numerical simulations.

ϕ_1 / V	ϕ_{-1}/ V	ϕ_3 / V	ϕ_4 / V	ϕ_5 / V	ϕ_{-5}/ V	ϕ_6 / V	ϕ_7 / V	β_5	k_2 / s^{-1}
−0.04	0.02	0.38	0.60	0.40	0.71	0.78	−0.40	0.65	1.1×10^2

Table 2
Constants used in the numerical simulations.

R_s / Ω	C_d / C V^{-1} cm^{-2}	A / cm^2	N_{tot} / mol cm^{-2}
10	24×10^{-6}	0.42	2.18×10^{-9}

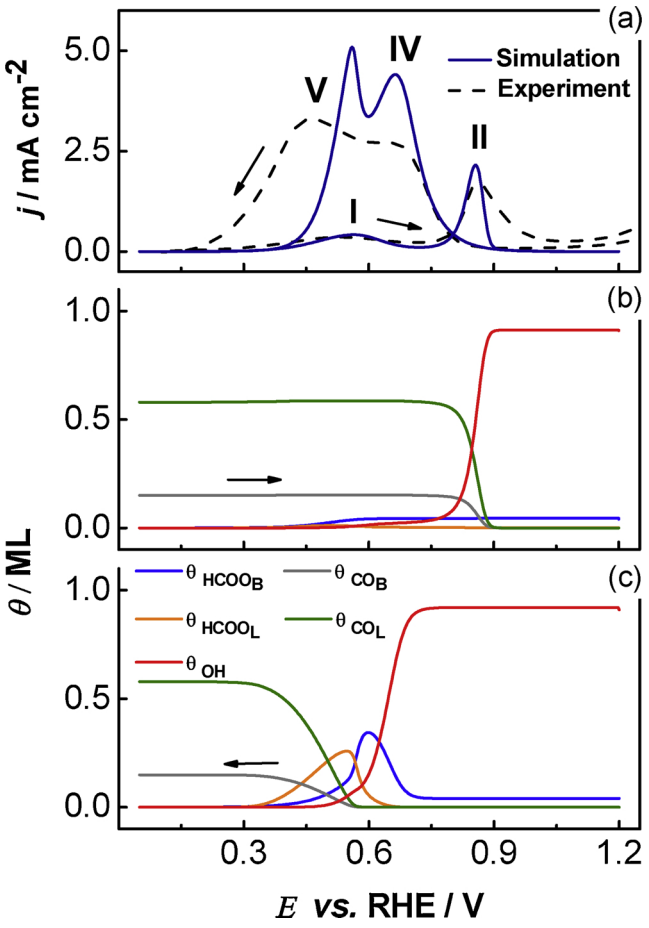

Fig. 4. (a) Voltammetry cyclic experiment of FAEOR; (b) coverage of adsorbates during a forward scan; and (c) coverage of adsorbates during a backward scan. [HCOOH] = 0.2 M; pH = 1.0; rate scan = 50 mV s^{-1}. Experimental results obtained from the reference [38]. The experiments were carried out in a solution containing 0.4 M K_2SO_4 + 0.2 M HCOOH of pH 1.02.

experiments or performed at very low scan rates [64].

However, at 50 mV s^{-1}, as in the case of the voltammetry of Fig. 4(a), the interplay of the adsorption/oxidation processes of CO_B, $HCOO_B$, and OH_{ad} affects the voltammetric profile. In this case, the intensity of peak I in the forward scan is affected by the increase in the coverage of adsorbates, as it is demonstrated in Fig. 4(b). As Samjeské et al. [15] found by ATR-SEIRAS, CO_{ad} adsorbs in a wide potential range between 0.0 and 0.70 V, where its high coverage drops rapidly to 0 due to its oxidation. After the oxidation of CO_{ad}, free platinum sites become available and allow the direct oxidation process, giving rise to peak II. As the IR data in the literature show [15], the coverage of $HCOO_B$ increases to a maximum at around 0.90 V. This is not the case in our simulation, where the $HCOO_B$ coverage remains approximately constant up to 1.2 V.

During the backward sweep, the peaks are more intense, since the electro-oxidation processes can take place ˜0.50 V on the platinum surface free of CO_{ads} [5,64]. Peak IV is associated with the process of oxidation of FA by the direct pathway, while peak V involves the formation of CO_2 both in the direct and formate pathways. Thus, the $HCOO_B$ coverage increase to its maximum at 0.60 V and decreases

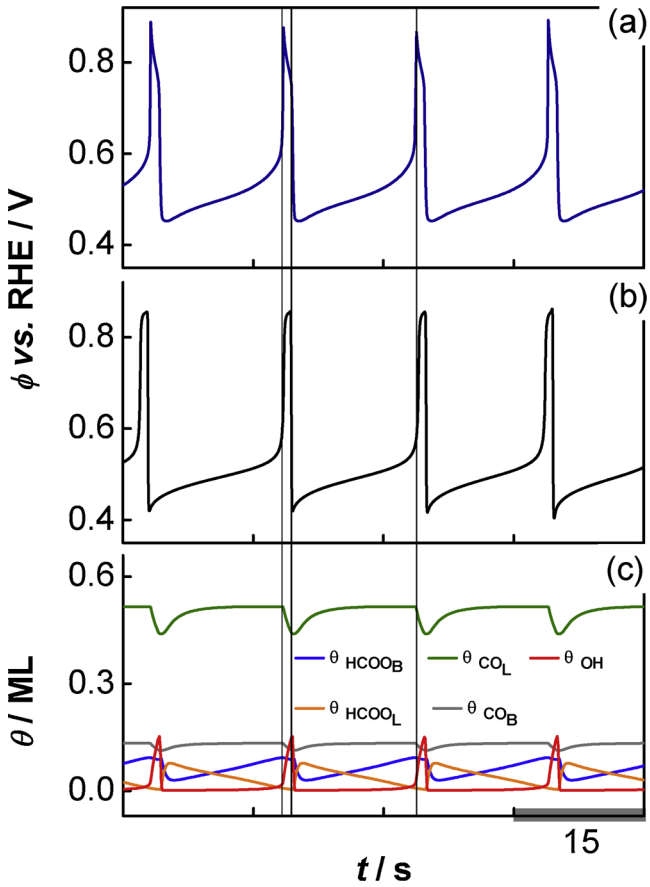

Fig. 5. (a) Simulated; and (b) Experimental potential time series during a galvanostatic experiment of formic acid oxidation; and (c) Simulated coverage of adsorbates during a galvanostatic experiment of formic acid oxidation: [HCOOH] = 0.2 M; pH = 1.0; j_{app} = 0.40 mA cm^{-2}. Experimental results obtained from the reference [38].

afterwards due to the formation of CO_{ad}, which is again in agreement with the data found by Osawa and coworkers [15]. Yet, it should be mentioned, that the simulated coverages do not mirror exactly the experimental data. This may be the consequence of a complex network of various surface processes like anion adsorption interfering in the oxidation of FA on platinum.

3.5. Kinetic instabilities

Simulated and experimental time-series of potential and coverage of adsorbates during a galvanostatic electro-oxidation of formic acid are shown in Fig. 5. A typical pattern is observed in which each cycle is characterized by an initial slow rise of potential followed by a sharp rise to high limiting value and sudden drop to low limiting value. These electrochemical oscillations in the galvanostatic oxidation of formic acid have been early explained in terms of oxidative removal of CO that inhibits and accelerates, respectively, the direct path [45]. However, the simulated results show that the coverage of all adsorbates oscillates synchronously with the potential. These results are consistent to experiments using EC-ATR-FTIRS by Osawa et al. [15–17].

Overall a very good agreement between simulated and experimental profiles has been provided, including the coverage of adsorbates previously reported [17]. Yet, there can be found some differences in the found patterns as well, when comparing simulations and experiments. As predicted by our model, the formate coverage increases constantly to its maximum close the potential spike and decreases afterwards first slightly with the slow decrease in the potential peak, then fast to its minimum, which appears close to the potential drop. In contrast, the

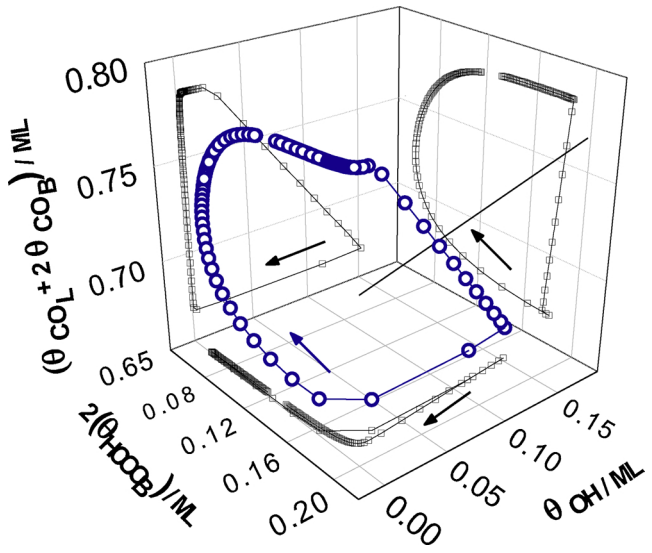

Fig. 6. Interplay of the coverage of the adsorbates during a galvanostatic experiment of formic acid oxidation: [HCOOH] = 0.2 M; pH = 1.0; j_{app} = 0.40 mA cm^{-2}.

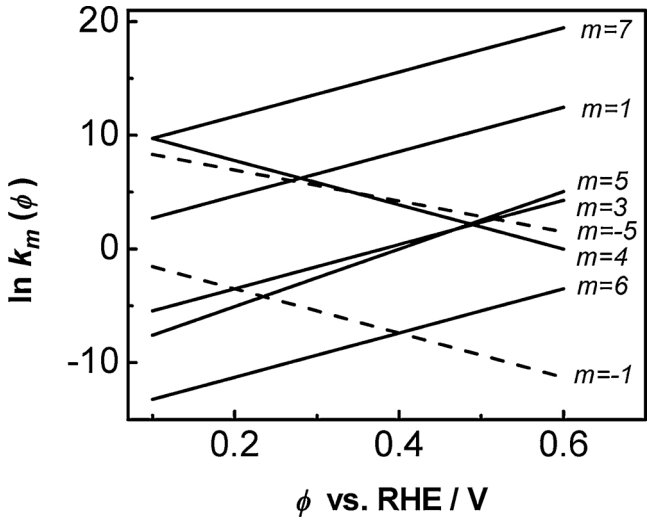

Fig. 7. Optimized rate constants obtained from numerical simulations with Eq. 10 as function of the electrode potential.

experiment shows the maximum in the formate coverage right before the potential drop, coinciding with the potential maximum and a following fast decrease with the potential to their minima [17,65]. Discrepancies can also be seen in the comparison to the simulations of Mei et al. [35], where the coverage of oxygenated species, which is not negligible in the low potential part of each oscillation cycle and show a non-zero coverage differently to our modeling. This fact suggests the presence of water on the Pt surface at any point of the time-series [35]. Here it should be emphasized that the coverage of oxygenated species and the potential increase synchronously until the potential peak, what suggests water as inhibiting species with respect to the direct oxidation pathway.

Fig. 6 shows the interplay of the coverage of different adsorbates along one cycle. The coverage of COL reaches the minimum value when the coverage of formate reaches its minimum. Then, the rapid oxidative removal of COad at $\phi >$ 0.8 V results in a small increase of the formate coverage and in an increase of the contribution to the applied current by direct pathway. After the drop of the potential to the potential minimum, the formate coverage decreases quickly to the initial value, while the COL recovers its coverage first quickly and then gradually [17]. The simulation also shows that, as in the case of formate, the coverage of the oxygenated species oscillates in phase with the potential, and in contrast to that for the coverage of CO. Thus, the coverage of OHad reaches the maximum value when the coverage of COad is minimum.

Recently published data [65] could give a deep insight of the Pt coverage of galvanostatic formic acid oxidation, where an intermediate level of CO_{ad} coverage was found along the potential oscillation cycle indicating a delay in the removal of CO_{ad} via Langmuir-Hinshelwood mechanism. The combination of ATR-SEIRAS and differential reflectance spectroscopy suggested that freed Pt sites due to CO_{ad} oxidation are occupied initially by sulfate rather than $HCOO_B$, which has a crucial impact in the interaction of CO_{ad} and OH_{ad}.

In conclusion, FAEOR takes place in a complex network of surface reactions, which may have a role in the oxidation mechanism or adsorb as spectator species occupying active surface sites. Consequently many adsorption processes have to be considered in FA oxidation on platinum, which makes an exact simulation of the voltammetric and galvanostatic response difficult. Nevertheless, this work is in line with many experimental observations reported in the literature so far [8,10–12,34,35], and for the first time, the voltammetric response is simulated in a wide range of potentials giving greater support to the proposed model. The use of realistic parameters, allows estimating the rate constants with greater certainty and reliability.

Nevertheless, the calculation of rate constants under standard conditions is not possible because the standard potentials of individual reaction steps are not known either. However, considering the aforementioned parameters it is possible to estimate the rate coefficients as a function of the electrode potential under conditions outside the steady state with a greater scope compared to previous works [48]. Table 3 presents values calculated using Eq. (10) for different electrode potentials ϕ. The complete set of rate constants as a function of the electrode potential is given in Fig. 7.

It is seen that the CO_2 formation is unequivocally faster by the direct pathway (*r7*) in comparison with the other two considered pathways. This observation has been reported in voltammetric studies as will be explained later [5,64]. In the same way, it is possible to observe that from the intermediate $HCOO_L$, the formation of CO_L (*r4*) is more kinetically favored than the CO_2 formation by *r3*. Therefore, it is expected that the formate pathway only has a significant contribution when the platinum surface has free sites and the *r6* reaction does not occur at an

Table 3
Optimized rate constants obtained from numerical simulations with Eq. 10 for selected values of the electrode potential.

ϕ / V	k_1 / $cm^3\ mol^{-1}\ s^{-1}$	k_{-1} / s^{-1}	k_3 / s^{-1}	k_4 / s^{-1}	k_5 / $cm^3\ mol^{-1}\ s^{-1}$	k_{-5} / s^{-1}	k_6 / s^{-1}	k_7 $cm^3\ mol^{-1}\ s^{-1}$
0.10	1.5×10^{1}	2.1×10^{-1}	4.3×10^{-3}	1.7×10^{4}	5.1×10^{-4}	4.1×10^{3}	1.8×10^{-6}	1.7×10^{4}
0.20	1.1×10^{2}	3.0×10^{-2}	3.0×10^{-2}	2.4×10^{3}	6.3×10^{-3}	1.0×10^{3}	1.3×10^{-5}	1.2×10^{5}
0.30	7.5×10^{2}	4.3×10^{-3}	2.1×10^{-1}	3.4×10^{2}	8.0×10^{-2}	2.7×10^{2}	8.8×10^{-5}	8.3×10^{5}
0.40	5.2×10^{3}	6.1×10^{-4}	1.5	4.9×10^{1}	1.0	6.8×10^{1}	6.1×10^{-4}	5.8×10^{6}
0.50	3.7×10^{4}	8.8×10^{-5}	1.0×10^{1}	7.0	1.3×10^{1}	1.7×10^{1}	4.3×10^{-3}	4.0×10^{7}
0.60	2.6×10^{5}	1.3×10^{-5}	7.2×10^{1}	1.0	1.6×10^{2}	4.5	3.0×10^{-2}	2.8×10^{8}

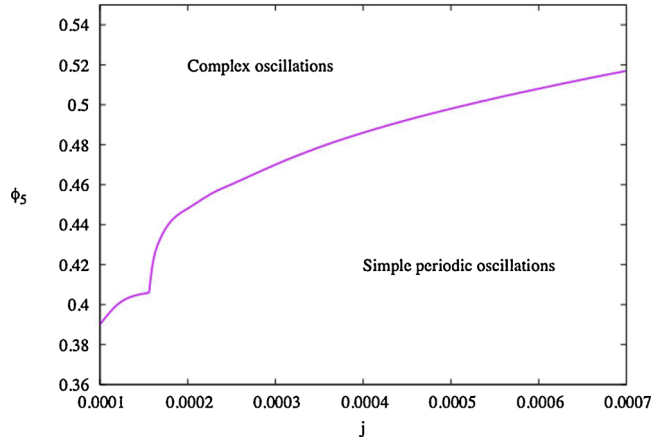

Fig. 8. Stability phase diagram indicating the nature of oscillations as predicted by Eqs. (11)–(15). Remaining parameters as in Table I and II.

appreciable rate, e.g. at E $<$ 0.8 V vs. RHE during the backward scan at voltammetry cyclic.

We have also estimated the dynamics over a wider parameter window. Out of the many possibilities we investigated the behavior in the j (j_{app}) vs. ϕ_5 plane, results are summarized in Fig. 8.

The kinetic model developed above was used to assess the nature and the relative abundance of the oscillatory patterns that it predicts. Fig. 8 shows a wide window in control parameter space where oscillations are expected. The dynamics of the model equations was investigated numerically by discretizing the window shown in Fig. 8 into a mesh of 200 × 200 equally spaced parameter points. Using a fourth-order Runge-Kutta integrator with fixed step $h = 5 \times 10^{-5}$, we recorded the temporal evolution obtained by starting integrations from the arbitrary initial condition (0, 0, 0, 0, 0), proceeding horizontally from left to right, and discarding a transient of 5×10^6 time-steps. The result of this investigation is the relatively smooth boundary curve separating the window in Fig. 8 into two distinct phases. For a fixed value of j, we observed a successive complexification of the oscillatory patterns as φ_5 increases towards the boundary. The upper region marked by complex oscillations is not a region of chaos but, instead, a region where one observes a slow and systematic amplitude drift of relatively regular oscillations. Clearly, such drifting oscillations are not periodic, although they may eventually evolve asymptotically to periodic oscillations with more complicated wave patterns. In this region, some of the variables did not oscillate, but displayed a linear increase or decrease as a function of time, while the other variables oscillated. The detailed investigation of both regions, of simple and complex oscillations, demands a considerable investment of computer time and, therefore, is postponed for a later opportunity.

4. Conclusions

In conclusion, we modeled the formic acid electro-oxidation reaction (FAEOR) on platinum and carried out numerical simulations under voltammetric and oscillatory regimes. The reaction mechanism proposed in this paper compiles a series of experimental and theoretical observations reported in the literature that the electro-oxidation of formic acid on platinum takes place mainly through a direct pathway that probably involves the participation of the formate anion instead of the formic acid, even in strongly acidic solutions. Both the formate and the indirect pathway take place through the change of configuration from the bridge-bonded formate to monodentate formate.

Almost all the Faradaic current observed during the cycle voltammetry corresponds to the process of oxidation of FA by direct pathway but the interplays of the adsorption/oxidation processes of CO_B, $HCOO_B$, and OH_{ad} affect the voltammetric profile and showing four current peaks at 50 mV s^{-1} in the window of potential studied. These interplays are also evaluated in galvanostatic conditions where potential oscillations and oscillations of the coverage of all adsorbates are observed. The good congruence of the numerical solution of our model, namely frequency and amplitude of the potential oscillations, with the experimental response makes our proposal a plausible possibility for the FAEOR, providing evidence to the clarification of this controversial process.

Acknowledgments

F.W.H. (grant #2014/08030-9) and HV (grants #2012/24152-1 and #2013/16930-7) acknowledge São Paulo Research Foundation (FAPESP) for financial support. HV (Grant No. 306060/2017-5) and JACG acknowledge Conselho Nacional de Desenvolvimento Científico e Tecnológico (CNPq) for financial support. This work was partially done in the framework of an Advanced Study Group on Forecasting with Lyapunov vectors, at the Max-Planck Institute for the Physics of Complex Systems, Dresden. This study was partially financed by the Coordenação de Aperfeiçoamento de Pessoal de Nível Superior – Brasil (CAPES) – Finance Code 001.

References

[1] S. Uhm, H.J. Lee, J. Lee, Understanding underlying processes in formic acid fuel cells, Phys. Chem. Chem. Phys. 11 (2009) 9326–9336, https://doi.org/10.1039/b909525j.
[2] E.R. Gonzalez, A. Mota-Lima, Direct Alcohol Fuel Cells, Springer Netherlands, Dordrecht, 2014, https://doi.org/10.1007/978-94-007-7708-8.
[3] T. Iwasita, Electrocatalysis of methanol oxidation, Electrochim. Acta 47 (2002) 3663–3674, https://doi.org/10.1016/S0013-4686(02)00336-5.
[4] K. Jiang, H.-X. Zhang, S. Zou, W.-B. Cai, Electrocatalysis of formic acid on palladium and platinum surfaces: from fundamental mechanisms to fuel cell applications, Phys. Chem. Chem. Phys. 16 (2014) 20360–20376, https://doi.org/10.1039/c4cp03151b.
[5] J. Joo, T. Uchida, A. Cuesta, M.T.M. Koper, M. Osawa, The effect of pH on the electrocatalytic oxidation of formic acid/formate on platinum: a mechanistic study by surface-enhanced infrared spectroscopy coupled with cyclic voltammetry, Electrochim. Acta 129 (2014) 127–136, https://doi.org/10.1016/j.electacta.2014.02.040.
[6] A. Cuesta, G. Cabello, M. Osawa, C. Gutiérrez, Mechanism of the electrocatalytic oxidation of formic acid on metals, ACS Catal. 2 (2012) 728–738, https://doi.org/10.1021/cs200661z.
[7] A. Cuesta, G. Cabello, C. Gutiérrez, M. Osawa, Adsorbed formate: the key intermediate in the oxidation of formic acid on platinum electrodes, Phys. Chem. Chem. Phys. 13 (2011) 20091–20095, https://doi.org/10.1039/c1cp22498k.
[8] M. Osawa, K.I. Komatsu, G. Samjeské, T. Uchida, T. Ikeshoji, A. Cuesta, C. Gutiérrez, The role of bridge-bonded adsorbed formate in the electrocatalytic oxidation of formic acid on platinum, Angew. Chemie - Int. Ed. 50 (2011) 1159–1163, https://doi.org/10.1002/anie.201004782.
[9] A. Cuesta, M.M. Escudero, B. Lanova, H. Baltruschat, Cyclic voltammetry, FTIRS, and DEMS study of the electrooxidation of carbon monoxide, formic acid, and methanol on cyanide-modified Pt(111) electrodes, Langmuir 25 (2009) 6500–6507, https://doi.org/10.1021/la8041154.
[10] Y.-X. Chen, M. Heinen, Z. Jusys, R.J. Behm, Kinetic isotope effects in complex reaction networks: formic acid electro-oxidation, ChemPhysChem. 8 (2007) 380–385, https://doi.org/10.1002/cphc.200600520.
[11] Y.X. Chen, M. Heinen, Z. Jusys, R.J. Behm, Kinetics and mechanism of the electrooxidation of formic acid—spectroelectrochemical studies in a flow cell, Angew. Chemie Int. Ed. 45 (2006) 981–985, https://doi.org/10.1002/anie.200502172.
[12] Y.-X. Chen, M. Heinen, Z. Jusys, R.J. Behm, Bridge-Bonded Formate: Active Intermediate or Spectator Species in Formic Acid Oxidation on a Pt Film Electrode? Langmuir. 22 (2006) 10399–10408, https://doi.org/10.1021/la060928q.
[13] Y.X. Chen, S. Ye, M. Heinen, Z. Jusys, M. Osawa, R.J. Behm, Application of in-situ attenuated total reflection-fourier transform infrared spectroscopy for the understanding of complex reaction mechanism and kinetics: formic acid oxidation on a pt film electrode at elevated temperatures, J. Phys. Chem. B 110 (2006) 9534–9544, https://doi.org/10.1021/jp057463h.
[14] W. Li, X. Wang, Z. Chen, M. Waje, Y. Yan, Pt-Ru supported on double-walled carbon nanotubes as high-performance anode catalysts for direct methanol fuel cells, J. Phys. Chem. B 110 (2006) 15353–15358, https://doi.org/10.1021/jp0623443.
[15] G. Samjeské, A. Miki, S. Ye, M. Osawa, Mechanistic study of electrocatalytic oxidation of formic acid at platinum in acidic solution by time-resolved surface-enhanced infrared absorption spectroscopy, J. Phys. Chem. B 110 (2006) 16559–16566, https://doi.org/10.1021/jp061891l.
[16] G. Samjeské, M. Osawa, Current oscillations during formic acid oxidation on a Pt electrode: insight into the mechanism by time-resolved IR spectroscopy, Angew. Chemie Int. Ed. 44 (2005) 5694–5698, https://doi.org/10.1002/anie.200501009.

[17] G. Samjeské, A. Miki, S. Ye, A. Yamakata, Y. Mukouyama, H. Okamoto, M. Osawa, Potential oscillations in galvanostatic electrooxidation of formic acid on platinum: a time-resolved surface-enhanced infrared study, J. Phys. Chem. B 109 (2005) 23509–23516, https://doi.org/10.1021/jp055220j.

[18] A. Ferre-Vilaplana, J.V. Perales-Rondón, C. Buso-Rogero, J.M. Feliu, E. Herrero, Formic acid oxidation on platinum electrodes: a detailed mechanism supported by experiments and calculations on well-defined surfaces, J. Mater. Chem. A 5 (2017) 21773–21784, https://doi.org/10.1039/C7TA07116G.

[19] K.A. Schwarz, R. Sundararaman, T.P. Moffat, T.C. Allison, Formic acid oxidation on platinum: a simple mechanistic study, Phys. Chem. Chem. Phys. 17 (2015) 20805–20813, https://doi.org/10.1039/C5CP03045E.

[20] W. Gao, E.H. Song, Q. Jiang, T. Jacob, Revealing the active intermediates in the oxidation of formic acid on Au and Pt(111), Chem. Eur. J. 20 (2014) 11005–11012, https://doi.org/10.1002/chem.201402737.

[21] W. Gao, J.A. Keith, J. Anton, T. Jacob, Theoretical elucidation of the competitive electro-oxidation mechanisms of formic acid on Pt(111), J. Am. Chem. Soc. 132 (2010) 18377–18385, https://doi.org/10.1021/ja1083317.

[22] H.-F. Wang, Z.-P. Liu, Formic acid oxidation at Pt/H2O interface from periodic DFT calculations integrated with a continuum solvation model, J. Phys. Chem. C 113 (2009) 17502–17508, https://doi.org/10.1021/jp9059888.

[23] A. Capon, R. Parsons, The oxidation of formic acid on noble metal electrodes II. A comparison of the behavior of pure electrodes, J. Electroanal. Chem. Interfacial Electrochem. 44 (1973) 239–254, https://doi.org/10.1016/S0022-0728(73)80250-5.

[24] A. Miki, S. Ye, M. Osawa, Surface-enhanced IR absorption on platinum nanoparticles: an application to real-time monitoring of electrocatalytic reactions, Chem. Commun. (2002) 1500–1501, https://doi.org/10.1039/b203392e.

[25] B. Beden, A. Bewick, C. Lamy, A study by electrochemically modulated infrared reflectance spectroscopy of the electrosorption of formic acid at a platinum electrode, J. Electroanal. Chem. 148 (1983) 147–160, https://doi.org/10.1016/S0022-0728(83)80137-5.

[26] K. Kunimatsu, H. Kita, Infrared spectroscopic study of methanol and formic acid absorbates on a platinum electrode, J. Electroanal. Chem. Interfacial Electrochem. 218 (1987) 155–172, https://doi.org/10.1016/0022-0728(87)87013-4.

[27] D.S. Corrigan, M.J. Weaver, Mechanisms of formic acid, methanol, and carbon monoxide electrooxidation at platinum as examined by single potential alteration infrared spectroscopy, J. Electroanal. Chem. Interfacial Electrochem. 241 (1988) 143–162, https://doi.org/10.1016/0022-0728(88)85123-4.

[28] Y. Mukouyama, M. Kikuchi, G. Samjeské, M. Osawa, H. Okamoto, Potential oscillations in galvanostatic electrooxidation of formic acid on platinum: a mathematical modeling and simulation, J. Phys. Chem. B 110 (2006) 11912–11917, https://doi.org/10.1021/jp061129j.

[29] V. Grozovski, V. Climent, E. Herrero, J.M. Feliu, Intrinsic activity and poisoning rate for HCOOH oxidation at Pt(100) and vicinal surfaces containing monoatomic (111) steps, ChemPhysChem 10 (2009) 1922–1926, https://doi.org/10.1002/cphc.200900261.

[30] V. Grozovski, F.J. Vidal-Iglesias, E. Herrero, J.M. Feliu, Adsorption of formate and its role as intermediate in formic acid oxidation on platinum electrodes, ChemPhysChem 12 (2011) 1641–1644, https://doi.org/10.1002/cphc.201100257.

[31] M. Neurock, M. Janik, A. Wieckowski, A first principles comparison of the mechanism and site requirements for the electrocatalytic oxidation of methanol and formic acid over Pt, Faraday Discuss. 140 (2009) 363–378, https://doi.org/10.1039/B804591G.

[32] J. Joo, T. Uchida, A. Cuesta, M.T.M. Koper, M. Osawa, Importance of acid–Base equilibrium in electrocatalytic oxidation of formic acid on platinum, J. Am. Chem. Soc. 135 (2013) 9991–9994, https://doi.org/10.1021/ja403578s.

[33] J. Xu, D. Yuan, F. Yang, D. Mei, Z. Zhang, Y.-X. Chen, On the mechanism of the direct pathway for formic acid oxidation at a Pt(111) electrode, Phys. Chem. Chem. Phys. 15 (2013) 4367–4376, https://doi.org/10.1039/c3cp44074e.

[34] J. Jiang, J. Scott, A. Wieckowski, Direct evidence of a triple-path mechanism of formate electrooxidation on Pt black in alkaline media at varying temperature. Part I: the electrochemical studies, Electrochim. Acta. 104 (2013) 124–133, https://doi.org/10.1016/j.electacta.2013.04.093.

[35] D. Mei, Z.-D. He, D.C. Jiang, J. Cai, Y. Chen, Modeling of potential oscillation during galvanostatic electrooxidation of formic acid at platinum electrode, J. Phys. Chem. C 118 (2014) 6335–6343, https://doi.org/10.1021/jp500285j.

[36] W. Gao, J.E. Mueller, Q. Jiang, T. Jacob, The role of Co-adsorbed CO and OH in the electrooxidation of formic acid on Pt(111), Angew. Chemie - Int. Ed. 51 (2012) 9448–9452, https://doi.org/10.1002/anie.201203078.

[37] J. John, H. Wang, E.D. Rus, H.D. Abruña, Mechanistic studies of formate oxidation on platinum in alkaline medium, J. Phys. Chem. C 116 (2012) 5810–5820, https://doi.org/10.1021/jp211887x.

[38] F.W. Hartl, H. Varela, The effect of solution pH and temperature on the oscillatory electro-oxidation of formic acid on platinum, ChemistrySelect 2 (2017) 8679–8685, https://doi.org/10.1002/slct.201702008.

[39] J.V. Perales-Rondón, E. Herrero, J.M. Feliu, Effects of the anion adsorption and pH on the formic acid oxidation reaction on Pt(111) electrodes, Electrochim. Acta 140 (2014) 511–517, https://doi.org/10.1016/j.electacta.2014.06.057.

[40] M.T.M. Koper, Combining experiment and theory for understanding electrocatalysis, J. Electroanal. Chem. 574 (2005) 375–386, https://doi.org/10.1016/j.jelechem.2003.12.040.

[41] M.T.M. Koper, Non-linear phenomena in electrochemical systems, Adv. Chem. Phys. 82 (1998) 161–298 doi:\url{10.1002/SERIES2007}.

[42] M.T.M. Koper, J.H. Sluyters, Instabilities and oscillations in simple models of electrocatalytic surface reactions, J. Electroanal. Chem. 371 (1994) 149–159, https://doi.org/10.1016/0022-0728(93)03248-N.

[43] P. Strasser, M. Eiswirth, G. Ertl, Oscillatory instabilities during formic acid oxidation on Pt(100), Pt(110) and Pt(111) under potentiostatic control. II. Model calculations, J. Chem. Phys. 107 (1997) 991–1003, https://doi.org/10.1063/1.474451.

[44] P. Strasser, M. Eiswirth, M.T.M. Koper, Mechanistic classification of electrochemical oscillators — an operational experimental strategy, J. Electroanal. Chem. 478 (1999) 50–66, https://doi.org/10.1016/S0022-0728(99)00412-X.

[45] F.N. Albahadily, M. Schell, Observation of several different temporal patterns in the oxidation of formic acid at a rotating platinum-disk electrode in an acidic medium, J. Electroanal. Chem. 308 (1991) 151–173, https://doi.org/10.1016/0022-0728(91)85064-V.

[46] H. Okamoto, N. Tanaka, M. Naito, Modelling temporal kinetic oscillations for electrochemical oxidation of formic acid on Pt, Chem. Phys. Lett. 248 (1996) 289–295, https://doi.org/10.1016/0009-2614(95)01295-8.

[47] M. Naito, H. Okamoto, N. Tanaka, Dynamics of potential oscillations in the electrochemical oxidation of formic acid on Pt, Phys. Chem. Chem. Phys. 2 (2000) 1193–1198, https://doi.org/10.1039/a908490h.

[48] M.R. Gennero de Chialvo, G.C. Luque, A.C. Chialvo, Formic acid electrooxidation on platinum, resolution of the kinetic mechanism in steady state and evaluation of the kinetic constants, ChemistrySelect 3 (2018) 9768–9772, https://doi.org/10.1002/slct.201801725.

[49] K. Krischer, H. Varela, Oxidation of small organic molecules: oscillations and other dynamic instabilities, in: W. Vielstich, A. Lamm, H.A. Gasteier (Eds.), Handb. Fuel Cells Fundam. Tecnol. Appl. Vol. 2 Fuel Cell Electrocatal, Wiley-VCH Verlag GmbH & Co. KGaA, Chichester, 2010, pp. 1–23.

[50] T. Gojuki, Y. Numata, Y. Mukouyama, H. Okamoto, Hidden negative differential resistance in the oxidation of formic acid on platinum, Electrochim. Acta 129 (2014) 142–151, https://doi.org/10.1016/j.electacta.2014.02.102.

[51] M. Naito, H. Okamoto, N. Tanaka, Dynamics of potential oscillations in the electrochemical oxidation of formic acid on Pt, Phys. Chem. Chem. Phys. 1198 (2000) 1193–1198.

[52] A. Cuesta, Formic acid oxidation on metal electrodes, Encycl. Interfacial Chem. Surf. Sci. Electrochem. Elsevier, 2017, pp. 620–632, https://doi.org/10.1016/B978-0-12-409547-2.13318-9.

[53] L.A. Kibler, M. Al-Shakran, Adsorption of formate on Au(111) in acid solution: relevance for electro-oxidation of formic acid, J. Phys. Chem. C. 120 (2016) 16238–16245, https://doi.org/10.1021/acs.jpcc.6b02044.

[54] W. Zhong, D. Zhang, New insight into the CO formation mechanism during formic acid oxidation on Pt(111), Catal. Commun. 29 (2012) 82–86, https://doi.org/10.1016/j.catcom.2012.09.002.

[55] W. Gao, J.A. Keith, J. Anton, T. Jacob, Oxidation of formic acid on the Pt(111) surface in the gas phase, Dalton Trans. 39 (2010) 8450, https://doi.org/10.1039/c0dt00404a.

[56] V. Grozovski, V. Climent, E. Herrero, J.M. Feliu, Intrinsic activity and poisoning rate for HCOOH oxidation on platinum stepped surfaces, Phys. Chem. Chem. Phys. 12 (2010) 8822, https://doi.org/10.1039/b925472b.

[57] G.-Q. Lu, A. Crown, A. Wieckowski, Formic acid decomposition on polycrystalline platinum and palladized platinum electrodes, J. Phys. Chem. B 103 (1999) 9700–9711, https://doi.org/10.1021/jp992297x.

[58] L.W. Liao, M.F. Li, J. Kang, D. Chen, Y.X. Chen, S. Ye, Electrode reaction induced pH change at the Pt electrode/electrolyte interface and its impact on electrode processes, J. Electroanal. Chem. 688 (2013) 207–215, https://doi.org/10.1016/j.jelechem.2012.08.031.

[59] H. Okamoto, Mechanistic studies of the potential oscillation and induction period in the oxidation of formic acid on platinum, Electrochim. Acta 37 (1992) 37–42, https://doi.org/10.1016/0013-4686(92)80009-B.

[60] Y. Tong, K. Cai, M. Wolf, R.K. Campen, Probing the electrooxidation of weakly adsorbed formic acid on Pt (1 0 0), Catal. Today 260 (2016) 66–71, https://doi.org/10.1016/j.cattod.2015.08.015.

[61] M.T.M. Koper, J.H. Sluyters, Electrochemical oscillators: their description through a mathematical model, J. Electroanal. Chem. 303 (1991) 73–94, https://doi.org/10.1016/0022-0728(91)85117-8.

[62] M.T.M. Koper, Non-linear phenomena in electrochemical systems, J. Chem. Soc. Faraday Trans. 94 (1998) 1369–1378, https://doi.org/10.1039/a708897c.

[63] A.J. Bard, R. Faulkner, Larry, Electrochemical Methods: Fundamentals and Applications, 2nd ed., John Wiley & Sons, Inc., New York, 2001.

[64] H. Okamoto, W. Kon, Y. Mukouyama, Stationary voltammogram for oxidation of formic acid on polycrystalline platinum, J. Phys. Chem. B 108 (2004) 4432–4438, https://doi.org/10.1021/jp031052o.

[65] F.W. Hartl, H. Varela, A. Cuesta, The oscillatory electro-oxidation of formic acid: insights on the adsorbates involved from time-resolved ATR-SEIRAS and UV reflectance experiments, J. Electroanal. Chem. 840 (2019) 249–254, https://doi.org/10.1016/j.jelechem.2019.04.015.